Journal of Molecular Catalysis A: Chemical 413 (2016) 67–76

Contents lists available at ScienceDirect

Journal of Molecular Catalysis A: Chemical

journal homepage: www.elsevier.com/locate/molcata

Monodisperse and polydisperse platinum nanoclusters supported over TiO_2 anatase as catalysts for catalytic oxidation of styrene

Mostafa Farrag

Chemistry Department, Faculty of Science, Assiut University, 71515 Assiut, Egypt

ARTICLE INFO

Article history:
Received 8 November 2015
Received in revised form 2 December 2015
Accepted 16 December 2015
Available online 22 December 2015

Keywords:
Monodisperse platinum nanoclusters
Non-protected platinum clusters
Oxidation of styrene
Doped TiO_2 anatase
Hydrogen peroxide

ABSTRACT

Very small platinum nanoclusters have been synthesized by reduction of $H_2PtCl_6{\cdot}6H_2O$ salt with $NaBH_4$ in the presence and absence of water-soluble L-cysteine ligand. The synthesized platinum clusters were supported over anatase titanium dioxide (TiO_2) by 1% wt/wt. The spectroscopic properties of Pt_n(L-Cys)$_m$ clusters were studied by UV–vis spectroscopy and Fourier transform infrared spectroscopy (FTIR) and its chemical structure were determined by thermogravimetric analysis (TGA) and elemental analysis. The particle sizes of supported and non-supported platinum clusters were characterized by transmission electron microscopy (TEM) and powder X-ray diffraction analysis. As well as their specific surface areas were determined using nitrogen adsorption/desorption measurements, pore volume and average pore diameter were also calculated. Finally, oxidation of styrene is used as a simple model reaction to demonstrate that these systems exhibit the potential to be used as heterogeneous catalysts. The doped monodisperse platinum clusters (1% Pt_n(L-Cys)$_m$/TiO_2) catalyst exhibited the highest catalytic activity and selectivity (100% benzaldehyde) in oxidation of styrene. The non-doped platinum clusters (Pt_n(L-Cys)$_m$) showed more catalytic activity than doped polydisperse platinum clusters (1% Pt/TiO_2). Hydrogen peroxide was used as oxidizing agent, which exhibited stronger oxidation potential than oxygen gas. The unique atom-packing structure and electronic properties of Pt_n(L-Cys)$_m$ nanoclusters (~1 nm) are rationalized to be responsible for their extraordinary catalytic activity observed in oxidation of styrene.

1. Introduction

Bulk platinum, as a noble metal, was initially thought to be catalytically inert, but the nanoparticles platinum (<10 nm) has been demonstrated to exhibit catalytic activity in a variety of chemical reactions [1–3]. However, the origin of the catalytic power of nanoscale platinum is still unclear and under intense debate [4]. This is primarily due to the polydispersity issue of platinum nanoparticles. To prepare monodisperse platinum clusters, a great deal of work on model catalysts should do, such as deposition of platinum atoms over single-crystal surfaces under ultrahigh vacuum (UHV) conditions 10^{-9} mbar [5]. This model of catalysis is very complicated and largely deviated from the real-world catalytic conditions.

I reported my effort in creating a well-defined catalytic system by preparing truly monodisperse, thiolate-capped gold nanoclusters (Au_n) [6–10] and protected platinum nanoclusters (Pt_n) [11–13] and utilizing them as homogeneous catalysts (unsupported) and heterogeneous catalysts (supported) for many chemical reaction such as selective oxidation and hydrogenation processes [4,14]. A colloidal method was used to prepare unprotected platinum clusters of well-defined size that are subsequently functionalized in a separate step with some hydrophilic chiral ligands [11]. These platinum clusters were supported over alumina to use as potential asymmetric catalysts in hydrogenation of 2-butanone [11]. Schrader et al. prepared Pt nanoparticles functionalized with L-proline ligand, these protected nanoparticles showed high catalytic activity in selective hydrogenation of acetophenone [12]. In my previous work, I synthesized some platinum nanoclusters protected by L-glutathione, *N*-acetyl-L-cysteine and L-penicillamine in regime ~1 nm [13]. These clusters showed high photocatalytic activity in degradation of methylene blue dye after deposition over Degussa TiO_2 P25 [13].

Different sizes of gold clusters ($Au_{25}(SCH_2CH_2Ph)_{18}$, $Au_{38}(SCH_2CH_2Ph)_{24}$ and $Au_{144}(SCH_2CH_2Ph)_{60}$) were used as catalysts in oxidation of styrene in presence of oxygen as oxidizing agent [4]. The catalytic activity of these clusters decreases in this order Au_{25} □ Au_{38} □ Au_{144} [15]. Coated titania with porous carbon (PC@TiO_2) showed the highest catalytic activity in oxidation of styrene compared to bare TiO_2 and carbon coated titania (C@TiO_2) in presence of hydrogen peroxide (H_2O_2) as oxidizing agent [16].

E-mail address: mostafafarrag@aun.edu.eg

http://dx.doi.org/10.1016/j.molcata.2015.12.011
1381-1169/

As we confirmed in our previous work [17] hydrogen peroxide is a stronger oxidizing agent than molecular oxygen. Size selected gold clusters protected by L-glutathione ($Au_{25}(SG)_{18}$) was supported over hydroxylapatite and calcined at 300 °C in vacuum 2 h to use as a catalyst in oxidization of styrene by using anhydrous *tert*-butyl hydroperoxide (TBHP) as an oxidant [18]. This catalyst oxidized styrene by 100% conversion and 92% selectivity to the epoxide after 12 h stirring [18]. Lambert and co-workers have demonstrated that Au_{55} clusters supported on silica (Au_{55}/SiO_2) can activate the catalytic oxidation reaction of styrene by using oxygen gas as oxidizing agent. This catalyst shows high catalytic conversion of styrene because of the electronic structures of the clusters, although the yield of the epoxide is not high (5%) [19]. This work hints at the possibility that there is an optimal cluster size for the efficient and selective oxidation of alkenes [19].

Herein, I report a new method to prepare monodisperse platinum clusters protected by L-cysteine. The method used in this work produces very narrow size distribution platinum clusters around 1 nm. The yield of prepared clusters is high, since this method based on a wet chemistry method. The optical properties of protected platinum clusters were studied by UV–vis spectroscopy and Fourier transform infrared spectroscopy (FTIR). The size and composition of Pt_n(L-Cys)$_m$ clusters were assessed by transmission electron microscopy (TEM), powder X-ray diffraction analysis (XRD), thermogravimetric analysis (TGA) and elemental analysis. The complete isotherm of the prepared clusters was measured using nitrogen adsorption–desorption at −196 °C, specific surface area S_{BET}, pore volume and average pore diameter were calculated. Powder X-ray diffraction analysis of protected clusters (unsupported) and supported platinum clusters over TiO_2 anatase were studied. To study the catalytic activity of synthesized cluster, oxidation of styrene is used as a model reaction to demonstrate that. Polydisperse platinum metal clusters over TiO_2 was prepared to comparison between the catalytic activity of monodisperse clusters and polydisperse clusters.

2. Experimental

2.1. Chemicals

Chloroplatinic acid ($H_2PtCl_6{\cdot}6H_2O$, ≥37.50% Pt basis, Sigma–Aldrich), Sodium borohydride ($NaBH_4$, ≥96%, Aldrich), L-cysteine (99%, Sigma–Aldrich) were used for synthesizing the protected platinum nanoclusters. Ethanol (HPLC grade, Sigma–Aldrich) was used to separate the nanoclusters from the aqueous mother solution. Styrene (99%, Sigma–Aldrich), hydrogen peroxide (H_2O_2) 30 wt.% in H_2O (Sigma–Aldrich) and oxygen gas were used in the catalytic reaction. Benzaldehyde (99%, Sigma–Aldrich), acetophenone (98%, Sigma–Aldrich) and styrene epoxide (97%, Sigma–Aldrich) were used as authentic samples. Titanium dioxide (TiO_2) anatase, 99.7% trace metals basis. All chemicals were used as received. All glassware was thoroughly cleaned with aqua regia (HCl:HNO_3 = 3:1 v/v), rinsed with 2nd distilled water and ethanol, and then dried in an oven prior to use.

2.2. Preparation of Pt_n(L-Cys)$_m$ nanoclusters

The 50 mg chloroplatinic acid ($H_2PtCl_6{\cdot}6H_2O$, 96 μmol) was dissolved in 10 ml 2nd distilled water, 7.8 mg L-cysteine (L-Cys, 65 μmol) was dissolved in 3 ml 2nd distilled water and added to the platinum solution, then vigorously stirring (~1100 rpm) at room temperature, the yellow solution of platinum salt showed some turbidity after adding the ligand, then the color changed to orange and finally to canaries yellow color. After 30 min stirring, freshly prepared aqueous solution of $NaBH_4$ (36.3 mg, dissolved in 2 ml 2nd distilled water) was added dropwise over the resulting solution while stirring vigorously (~1100 rpm), During the reduction step the color of solution changed from canaries yellow to brown then to deep brown gradually, indicating the reduction of the platinum salt and the formation of nanoparticles. The reaction was allowed to proceed under constant stirring for 1 h. The mixture was evaporated under a vacuum to near dryness, and then the particles were precipitated by adding ethanol. The resulting precipitate was then collected through centrifugal precipitation and repeatedly washed with ethanol to remove the unreacted material. The deep brown solid consisting of Pt_n(L-Cys)$_m$ nanoclusters was finally dried under reduced pressure in a vacuum desiccator.

2.3. Preparation of supported Pt_n(L-Cys)$_m$ nanoclusters over TiO_2 anatase

The 1% Pt_n(L-Cys)$_m/TiO_2$ catalyst was prepared by well known impregnation method. 1 g TiO_2 anatase powder was dispersed into a 40 ml aqueous solution contains 10 mg Pt_n(L-Cys)$_m$ clusters. The slurry was stirred one day at room temperature, the brown color of clusters solution becomes colorless, confirming the transfer of all clusters amount to the TiO_2 surface. The suspension was evaporated at 100 °C until drying, getting size selected nanoclusters supported over TiO_2, denoted as 1% Pt_n(L-Cys)$_m/TiO_2$.

2.4. Preparation of polydisperse platinum clusters over TiO_2

(I) A 1 g of TiO_2 anatase was dispersed in 30 ml of water, and then 10 mg of $H_2PtCl_6{\cdot}6H_2O$ dissolved in 10 ml water was added to the suspension. Such mixture was stirred one day at room temperature, filtered, washed, and then dried at 100 °C.

(II) 20 ml of 5 mg/ml $NaBH_4$ aqueous solution was added to 100 mg of as-prepared powder (from first step). The mixture was stirred at room temperature for 60 min, filtered, washed, and then dried at 100 °C overnight, getting nanoparticles, denoted as 1% Pt/TiO_2.

2.5. Catalytic oxidation of styrene

100 mg powder from the supported platinum catalysts (1% Pt_n(L-Cys)$_m/TiO_2$ and 1% Pt/TiO_2) and the bare support material (TiO_2 anatase) or 1 mg of unsupported platinum clusters (Pt_n(L-Cys)$_m$) were mixed with 20 ml styrene solution in toluene (40 mM), then the oxidizing agent was added in a 50 ml round bottom flask with vigorous stirring. I used three types of oxidizing agents (1) 0.5 ml of hydrogen peroxide (2) 7.5 μl hydrogen peroxide (as initiator) and pure O_2 gas (as oxidizing agent) (3) pure O_2 gas (99.99%). Then the mixture was heated to 80 °C for 12 h. To follow up the conversion of styrene during the stirring time, several cuts were extracted every one hour, and then the decreasing in the styrene concentration and the yield of products were detected by gas chromatography after removing the catalysts by filtration. I identified the products by authentic samples and gas chromatography/mass spectrophotometer (GC/MS).

2.6. Instrumentation and characterization

To obtain the UV–vis absorption spectra of the platinum clusters (Pt_n(L-Cys)$_m$) and bare ligand (L-cysteine), aqueous solution of approximately 1–2 mg/ml was prepared. The spectra were recorded at ambient temperature from 200 to 800 nm with a double-beam spectrophotometer (Evolution 300). Thermal gravimetric analysis (TGA, ~ 2 mg sample tested) was conducted in a N_2 atmosphere (flow rate ~50 ml /min) with a ThermoStartTM TG/DAT (Pfeiffer Vacuum). The measurement was performed with a heating rate of 10 °C/min, starting from room temperature and ramping

up to 1000 °C. Analysis of C, S, N, and H content was performed by an elemental analyzer (Vario EL) that allowed controlled combustion of the samples with subsequent chromatographic separation and the detection of the as-separated species with a TCD detector. The amount of Pt was analyzed by a fast sequential atomic absorption spectrometer (ICAP 6200 ICP-OES analyzer—Thermo Scientific) using a Pt lamp as light source. PtNCs were dissolved in aqua regia, and the solution was then evaporated completely. The sample was re-dissolved in 10% HCl. For calibration, Pt solutions of different concentrations were prepared using the standard matrix. For TEM measurements, solutions with a concentration of 1–2 mg/ml were prepared by dissolving or suspension the catalysts materials in 2nd distilled water. A droplet of these catalysts solutions was casted onto carbon-coated copper grids. The solvent was then allowed to evaporate slowly. TEM images were obtained at a magnification of 300,000, 200,000, 150,000 and 30,000 for 1% Pt_n(L-Cys)$_m$/TiO_2, Pt_n(L-Cys)$_m$ clusters, 1% Pt/TiO_2 and TiO_2 anatase samples, respectively, with a high resolution transmission electron microscope (HRTEM) TECNAI G^2 spirit TWIN at acceleration voltage of 120 kV, conducted by VELETA Camera. The images were then analyzed by using Image J software (version 1.44). Powder X-ray diffraction (XRD) was performed on a philips X-ray powder diffractometer, model pw 2013/00. Ni-filtered Cu Kα with a wavelength of λ = 1.541838 Å was used as a constant source of radiation. The generator was operated at 35 kV and 20 mA, and diffractometer at 50 diverting and receiving slits and a scan rate of 20 mm/min. Fine powder samples were loaded on a quartz plate holder by spreading the powders as a smooth thin layer on the plate. For all diffractograms, the following settings were used: scan range 4–80° (2θ), scan step 0.06°. Infrared spectra of all protected clusters and the ligands were obtained using an FTIR spectrometer (Nicolet iS10, resolution: 4 cm^{-1}, Thermo Scientific corporation, transmission mode) using KBr disks. Each spectrum was obtained by accumulating 200 scans. The system which investigates the textural studies of the samples is of the type NOVA 3000, version 6.10 high-speed gas sorption analyzer (Quantachrome corporation). Prior to analysis, the samples were outgases at 150 °C for 2 h. Five points BET surface areas, total pore volumes, and pore size distribution (BJH method) were calculated from 24 points nitrogen adsorption–desorption isotherms. GC analysis was performed employing Thermo Scientific, Trace GC ultra using capillary column TG-5MS (5% Phenyl Methylpolysiloxane), length 30 m, internal diameter 0.25 mm, and film thickness 0.25 μm. The initial temperature of column is 50 °C and the final temperature is 300 °C, the rate of heating is 10 °C/min. The injector temperature is 350 °C and the detector temperature is 350 °C, flame ionization detector is the used detector. GC/MS analysis were carried out by GC model: GC 7890A, using capillary column DB-5 ms (5% phenyl—95% methyl polysiloxane), with length 30 m, internal diameter 0.25 mm, film thickness 0.5 μm, initial temperature of column 50 °C, final temperature 300 °C, rate of heating 10 °C/min. and injector temperature 250 °C, attached with mass spectrometer: model 5975B.

3. Results and discussion

In the following I present an approach for obtaining size selected platinum clusters functionalized with L-cysteine ligand. After having successfully synthesized the monolayer-protected platinum nanoclusters, the sample was characterized by UV–vis spectroscopy, Fourier transform infrared (FTIR), transmission electron microscopy (TEM), X-ray diffraction (XRD), thermogravimetric analysis (TGA) and surface area measurements. The catalytic activity of the synthesized clusters and supported platinum clusters over TiO_2 anatase was evaluated for oxidation of styrene.

Table 1
Elementals ratios of Pt_n(L-Cys)$_m$ clusters were determined by elemental analysis (EA) and atomic absorption spectroscopy (AAS).

Elements	C	H	N	S	O	Pt
Percentage	7.8	1.85	3.06	6.89	11.39	69.01

3.1. Chemical composition of protected platinum nanoclusters (Pt_n(L-Cys)$_m$)

The effective ways to obtain the ratio between organic part and the metal content is elemental analysis and thermogravimetric analysis. With this technique the metal-to-ligand ratio (M/L) and, hence, the average chemical formula of the protected nanoclusters (PNCs) can be determined. TGA curve of protecting ligand (L-cysteine) shows several decomposition steps (Fig. 1b) [9]. Fig. 1a shows the thermogram of Pt_n(L-Cys)$_m$ nanoclusters, the clusters are found to be hygroscopic, which is indicated by the early detected mass loss at 29 °C. A mass loss at this low temperature is attributed to the removal of adsorbed water molecules rather than to a decomposition of the ligand, since the pure ligand does not show any mass loss up to 200 °C [9,20]. The other steps of the TGA curve correspond to the decomposition of the protecting ligand. The decomposition of the ligand is completed before 1000 °C and the residue consists of platinum metal atoms only (Table S1 and Fig. 1a).

From the relative weight of the residue and the total weight loss of organic ligand, the average metal-to-ligand ratio (M/L) can be calculated and thus the average molecular formula of the synthesized clusters is derived as $Pt_{3n}L_{2n}$ (Table S1) [9,20,21]. The size selected gold and silver clusters $Au_{25}(SCH_2CH_2Ph)_{18}$ [6] and Ag_{25}(L-GSH)$_{18}$ [9] showed the same metal to ligand ratio.

TGA analysis shows that the organic weight loss of the platinum nanoclusters is 30.97% (wt.). Therefore, the platinum content of Pt_n(L-Cys)$_m$ clusters is calculated as 69.03% (Tables S1). This composition is further supported by the elemental analysis of the Pt_n(L-Cys)$_m$ nanoclusters, which show that the organic content of these clusters consists of 7.8% C, 1.85% H, 3.06% N, 6.89% S and 11.39% O (sum 30.99% wt.) (Table 1). In addition, by using atomic absorption spectroscopy, the percentage of Pt was directly obtained. It was found to be 69.01% (Table 1), thus confirming composition obtained from thermogravimetric analysis [20].

3.2. Optical properties of protected platinum manoclusters (Pt_n(L-Cys)$_m$)

The origin of optical properties for protected metal clusters comes from the excitation of electrons plasmon resonance or interband transitions, the region and number of absorbance are characteristic for each metal, particles size, chemical valence and protected ligand.

The platinum nanoclusters protected by different ligands in regime 3–20 nm show absorption band at 215 nm [22,23]. However, the intensity of this band decreases rapidly for particles smaller than 3 nm, and is essentially undetectable for smaller clusters less than 2 nm [24]. Fig. 2a shows the UV–vis absorption spectrum of the synthesized platinum clusters (Pt_n(L-Cys)$_m$). This spectrum shows featureless absorption curve in visible regions, in agreement with its brown color. The capping agent (L-cysteine) shows one absorption peak at 2 1 0 nm (Fig. 2b). The disappearance of ligand peak in the UV–vis spectrum of protected clusters (Fig. 2a), confirm the prepared clusters are completely pure from the unreacted ligand.

The ligand anchors to the cluster surface through the sulfur atom [13,20], this confirmed by Infra-red (IR) analysis (Fig. S1). By comparing the IR absorption spectrum of pure ligand with those of the platinum clusters, the vibrational band of the S—H function group at

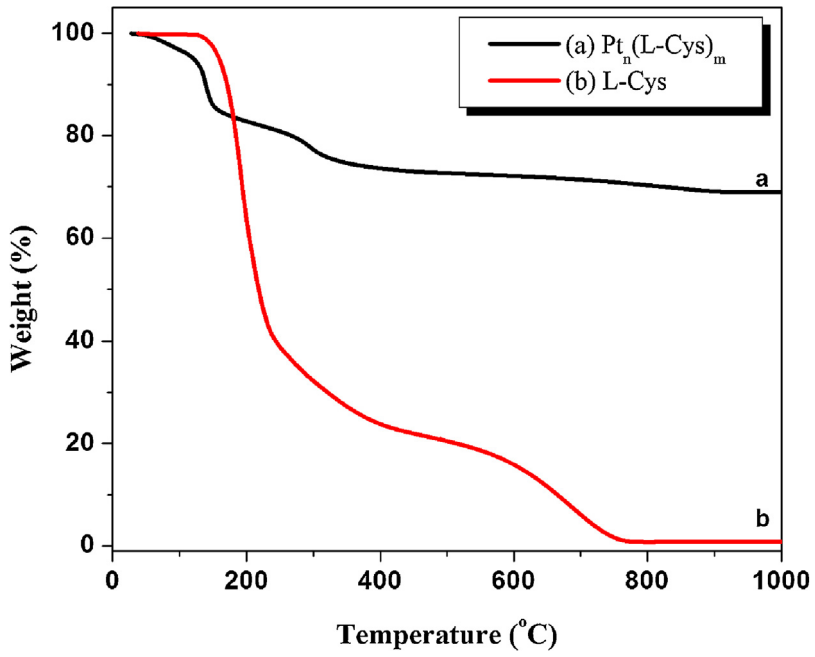

Fig. 1. The thermogravimetric analysis of synthesized platinum clusters Pt_n(L-Cys)$_m$ (curve a) and protecting ligand L-cysteine (curve b).

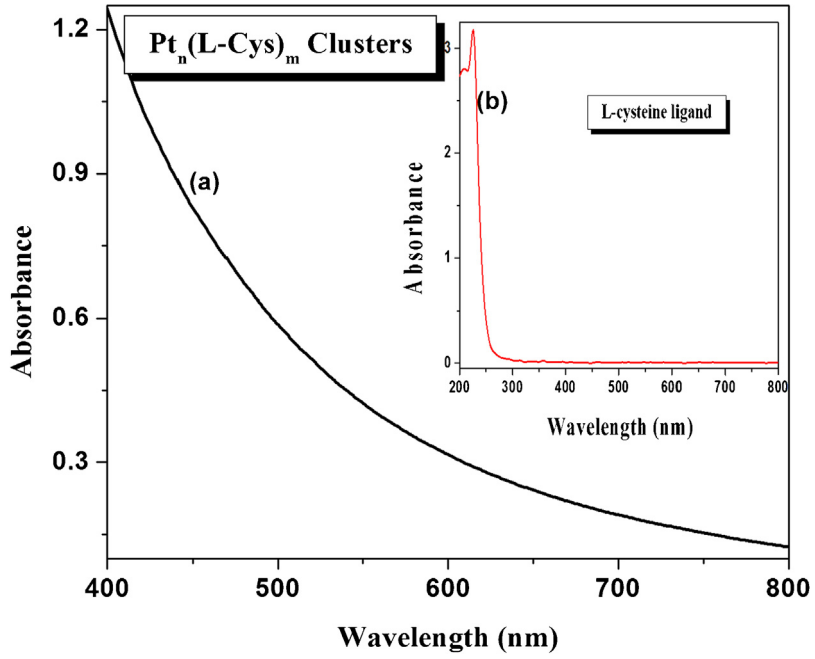

Fig. 2. UV–vis absorption spectrum of synthesized platinum clusters Pt_n(L-Cys)$_m$ (curve a) and protecting ligand L-cysteine (curve b). Pt_n(L-Cys)$_m$ clusters shows featureless absorption curves in UV and visible region 200–800 nm and L-cysteine ligand shows one absorption peak at 2 1 0 nm.

2535–2564 cm^{-1} in the protected clusters disappears (Fig. 1S), confirming the anchoring of ligand to the cluster surface through the sulfur atom [13,20,25]. However, the rest of ligand bands appeared in the same position with the protected clusters, but with low intensity. This confirms the chemical structure of the capping ligands did not change in protected clusters.

3.3. Particles size of synthesized platinum clusters.

To determine the particle size of the synthesized catalysts Pt_n(L-Cys)$_m$, 1% Pt_n(L-Cys)$_m$/TiO_2, 1% Pt/TiO_2 and bare TiO_2 anatase, two analytical methods were applied transmission electron microscopy (TEM) (Fig. 3) and powder X-ray diffraction (XRD) analysis (Fig. 4). TEM is particularly suited for obtaining the sizes of particles larger than 1 nm. It is found that, the particles of Pt_n(L-Cys)$_m$ clusters are uniformly distributed and have a diameter of about 1 nm (Fig. 3-I). This is a clear indication that particles with a very narrow size distribution can be obtained with this synthesis method. According to the TEM image (Fig. 3-I) I expect, the synthesized nanoparticles are monodisperse clusters, especially this image is similar to Au_{25} clusters protected by 2-phenylethanethiol [6] and L-glutathione [9]. However, the particle size distribution of Pt_n(L-Cys)$_m$ clusters was measured using image J program. Around 70 particles have size 1 nm and the rest 33 particles have size 1 ± 0.1 nm (Fig. 3-I).

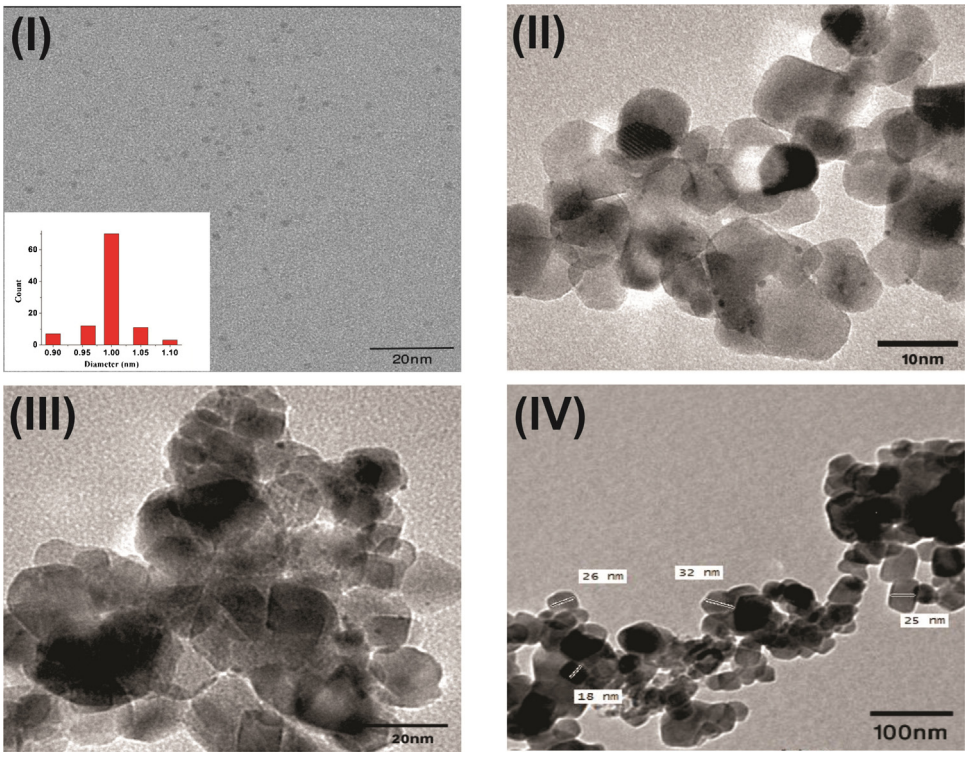

Fig. 3. Transmission electron microscopy (TEM) images (I–IV) of synthesized platinum clusters Pt_n(L-Cys)$_m$ (~1 nm), 1% Pt_n(L-Cys)$_m$/TiO_2, non-protected platinum clusters over TiO_2 (1% Pt/TiO_2, 2 ± 0.5 nm) and TiO_2 anatase (av. 25 nm), respectively.

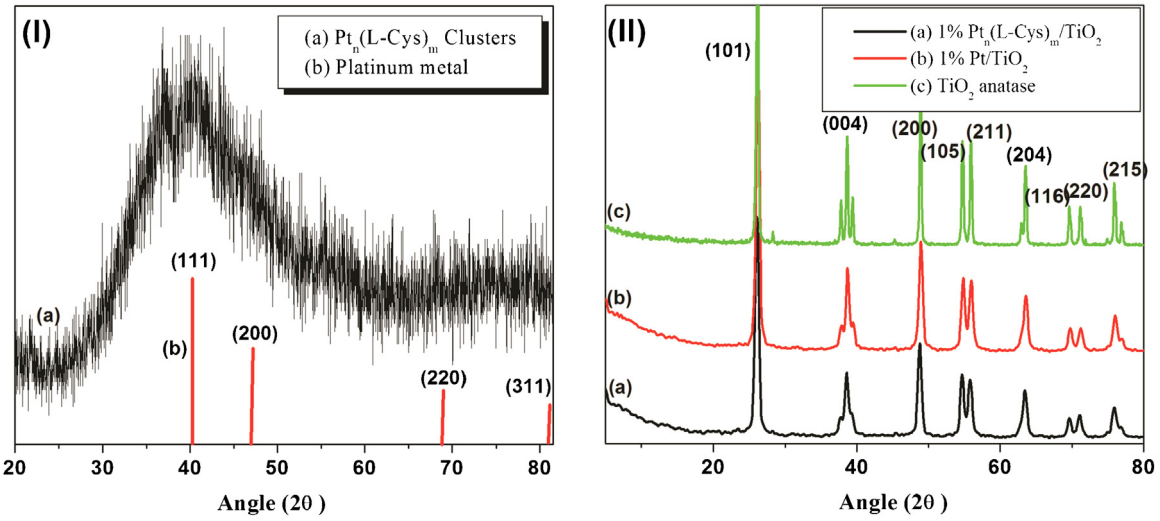

Fig. 4. (I) X-ray diffractograms of Pt_n(L-Cys)$_m$ clusters (curve a), which exhibits a broad and intense (1 1 1) peak of platinum at $2\theta = \sim 40^\circ$ and the stick pattern (curve b) is an indication of the diffraction peaks of the bulk Pt metal, which shows face-centered cubic (fcc) lattice (1 1 1), (2 0 0), (2 2 0), and (3 1 1) reflections. (II) X-ray diffractograms of 1% Pt_n(L-Cys)$_m$/TiO_2, 1% Pt/TiO_2 and TiO_2 catalysts (curves a–c), respectively.

TEM analysis was used to confirm the Pt_n(L-Cys)$_m$ clusters after deposition over TiO_2 anatase still monodisperse and do not agglomerate (Fig. 3-II). However, reduction of deposited platinum salt over TiO_2 by sodium borohydride in absence of L-cysteine ligand produces polydisperse platinum clusters in regime 2 ± 0.5 nm as seen in image Fig. 3-III., this refer to the role of protecting ligands in produce monodisperse clusters. Fig. 3-IV shows the particles size of the bare TiO_2 anatase in average 25 nm.

Powder X-ray diffraction (XRD) was used to compare the structures of the synthesized platinum nanoclusters protected by L-cysteine with that of bulk platinum (Fig. 4-I). The X-ray diffractogram of Pt_n(L-Cys)$_m$ powder (Fig. 4-Ia) exhibits a broad and intense feature at $2\theta = 40 \pm 0.5^\circ$, which is centered at almost the same position as the peak of a bulk platinum (1 1 1) lattice (Fig. 4-Ib) [26,27]. Fig. 4-Ib shows the diffraction pattern of bulk platinum metal (stick spectrum), which shows face-centered cubic (fcc) lattice 40° (1 1 1), 46.5° (2 0 0), 67.5° (2 2 0) and 81° (3 1 1) reflections [26,27].

The particles size of the synthesized platinum nanoclusters Pt_n(L-Cys)$_m$ can be estimated according to the broadening of the full width at half-maximum (fwhm) of the (1 1 1) diffraction peak by the Debye–Scherrer equation [9]. The calculated particles size of Pt_n(L-Cys)$_m$ clusters from XRD analysis is 0.9 ± 0.05 nm, which in good agreement with TEM analysis. According to the Bragg equa-

tion, this broad and intense peak indicates an average interplane spacing (d) of 2.255 ± 0.025 Å, which corresponds very well to the interplane spacing of bulk Pt (1 1 1) 2.25 Å.

Fig. 4-II illustrates XRD diffractograms of 1% Pt_n(L-Cys)$_m$/TiO_2, 1% Pt/TiO_2 and TiO_2 anatase catalysts. The characteristic diffractions peaks of TiO_2 anatase are (1 0 1), (0 0 4), (2 0 0), (1 0 5), (2 0 4), (1 1 6), (2 2 0) and (2 1 5) appear at 2θ equal to 25.35°, 37.78°, 47.5°, 53.92°, 62.72°, 68.99°, 74.49°, 82.21°, respectively (Fig. 4-IIc) [28]. Doping TiO_2 by Pt_n(L-Cys)$_m$ clusters and polydisperse platinum clusters do not modify its pattern and no other peaks related to the presence of Pt are detected (Fig. 4-IIa and b, respectively). The only different between the diffractogram of bare TiO_2 and platinum doped TiO_2 is relatively wider and lower intense peaks with doped catalysts. This indicates a little distortion in the crystalline structure of the bare TiO_2 was happened, because the location of platinum clusters within the TiO_2 lattice is not possible owing to the mismatch of ionic radius between TiO_2 and platinum [29]. The crystalline size (d_{TiO2}) of bare TiO_2 anatase is calculated by using Debye–Scherrer equation as 28 nm for the broadening of (1 0 1) peak reflection. The d_{TiO2} values in 1% Pt_n(L-Cys)$_m$/TiO_2 and 1% Pt/TiO_2 catalysts are less than bare TiO_2 16 and 17.2 nm, respectively.

3.4. Texture analysis of synthesized platinum clusters

The surface texture properties of Pt_n(L-Cys)$_m$, 1% Pt_n(L-Cys)$_m$/TiO_2 and 1% Pt/TiO_2 catalysts, as well as the bare TiO_2 anatase for comparison were studied by measuring the adsorption–desorption isotherms (Fig. 5).

The adsorption–desorption isotherms of bare TiO_2 anatase and 1% Pt/TiO_2 show large hysteresis loops characterizing mesoporous nature of H1 type (Fig. 5-IIa and b, respectively). However, unsupported clusters (Pt_n(L-Cys)$_m$) and the doped TiO_2 with this clusters (1% Pt_n(L-Cys)$_m$/TiO_2) show sorption isotherm from type H4 and H3 (Fig. 5-Ia and b, respectively) according to IUPAC classification of hysteresis loops [30].

The specific surface area and pore volume distribution of all catalysts are summarized in Table 2. As I mentioned before in XRD analysis, the doped metal creates defect sites and surface disorder in the support (TiO_2), therefore the total pore volume of doped alumina (1% Pt/TiO_2) is more than the bare TiO_2 [29]. In concordance, the doped titania with Pt_n(L-Cys)$_m$ clusters shows decrease in pore volume, since the particles size of these clusters are very small (~1 nm), therefore localized deep inside the pores affecting the pore volumes that by its turn decrease the surface area values (Table 2). Therefore, This explain why the hysteresis loop of non-doped TiO_2 changed from H1 into H3 type by doping with protected platinum clusters and keeps H1 type when doped by non-protected platinum clusters (1% Pt/TiO_2).

The pore size distributions of all catalysts were determined by the BJH method (Fig. 5-III). The results showed that the pore size of TiO_2 anatase was uniform in two domains maximizing at 185.4 and 22.7 Å; as a broad and sharp bands, respectively (Fig. 5-IIIc), also the doped catalyst (1% Pt/TiO_2) showed two maximum peaks at 235.5 and 20.1 Å (Fig. 5-IIId), whereas the Pt_n(L-Cys)$_m$ and 1% Pt_n(L-Cys)$_m$/TiO_2 catalysts showed a one sharp maximum peak at ~27 Å (Fig. 5-IIIa and b, respectively). Fig. 5-III shows the 1% Pt/TiO_2 and bare TiO_2 catalysts have mesoporous and small number from micropores, however, Pt_n(L-Cys)$_m$ and 1% Pt_n(L-Cys)$_m$/TiO_2 catalysts have only micropores. The V_{a-t} plots of Pt_n(L-Cys)$_m$ and 1% Pt_n(L-Cys)$_m$/TiO_2 catalysts exhibited a downward deviation (Fig. 5-IVa and b), this clearly suggests the presence microporous nature in these two catalysts. However, 1% Pt/TiO_2 and bare TiO_2 catalysts exhibited upward deviation (Fig. 5-IVc and d) confirming the presence of mesoporous. Therefore, I can say the V_{a-t} calculation in good agreement with the pore size calculation by the BJH method.

Table 2 gives the textural data obtained through the analysis of N_2 sorption data of all prepared catalysts. The values of S_{BET} and S_t for all investigated clusters are close to each other which justify the correct choice of standard *t*-curves for pore analysis and indicate the absence of ultra-micropores in this adsorbents [31,32].

3.5. Catalytic activity of synthesized platinum clusters

Herein, I chose selective oxidation of styrene by using hydrogen peroxide and/or oxygen gas as oxidizing agents to test the utility of platinum nanoclusters as oxidation catalysts. The process of selective oxidation of styrene is of industrial importance, since the products of styrene oxidation (benzaldehyde, styrene epoxide and acetophenone) are high-value chemicals widely used in fine chemical industry (Scheme 1).

To elucidate the effects of particle sizes of platinum nanoclusters and the effects of supports, monodisperse and polydisperse platinum nanoclusters were prepared and supported over TiO_2 anatase. I chose three oxidant systems to oxidize styrene: (1) hydrogen peroxide (H_2O_2) as the oxidant, (2) H_2O_2 as an initiator and O_2 as the main oxidant, and (3) O_2 as the oxidant. The temperature of this catalytic reaction is 80 °C, below the thiolate-desorption onset temperature of Pt_n(L-Cys)$_m$ clusters (Fig. 1), I believe that the thiolate ligands should remain on the protected clusters during the course of the catalytic reaction. The catalytic reaction occurs at the surface of metal clusters, whereas the molecules of styrene is small and can penetrate the thiolate ligand shell of Pt_n(L-Cys)$_m$ and reach to the cluster surface [33].

Firstly, I studied the effect of catalyst size and the effect of support in the catalytic oxidation of styrene by using one type of oxidizing agent (H_2O_2). The catalytic activity of platinum clusters catalysts exhibits a strong dependence on size. The smaller platinum clusters (Pt_n(L-Cys)$_m$, ~1 nm) shows a much higher catalytic activity than the polydisperse clusters 2 ± 0.5 nm (Fig. 6-I). Moreover, supporting of monodisperse clusters (Pt_n(L-Cys)$_m$) over TiO_2 (1% Pt_n(L-Cys)$_m$/TiO_2) leads to large increase in catalytic activity of styrene compared to 1% Pt/TiO_2 and unsupported Pt_n(L-Cys)$_m$ catalysts (Fig. 6-I). This increasing in activity attributed to the electronic interaction between TiO_2 and Pt_n(L-Cys)$_m$ and increase of the exposed area from clusters to the reaction after deposition over the support (TiO_2) [14,15]. However, the bare TiO_2 does not catalyze the styrene oxidation reaction under comparable conditions (Fig. 6-I). The good linear correlation of (Ln C_o/C) versus stirring time plot is the proof for the pseudo-first order rate kinetics (Fig. 6-II). To determine the role of support (TiO_2) in catalytic oxidation of styrene, the activation energy (E_a) was calculated. The values of rate constants measured at 70–100 °C over 1% Pt_n(L-Cys)$_m$/TiO_2 and Pt_n(L-Cys)$_m$ catalysts have been used to calculate the activation energy values by applying Arrhenius equation (Fig. 6-III). The activation energy of styrene oxidation using H_2O_2 as oxidizing agent over 1% Pt_n(L-Cys)$_m$/TiO_2 and Pt_n(L-Cys)$_m$ catalysts are 57.16 and 70.15 KJ/mol, respectively. From the activation energy values the support (TiO_2) reduces the required energy to activate this reaction. Thus I can say the role of support is not only better disperse of platinum clusters but also reduce activation energy of styrene oxidation reaction by the electronic interaction between TiO_2 and Pt_n(L-Cys)$_m$ clusters. This result is in good agreement with the previous published work [4,14,15,34–36], in selective hydrogenation of benzalacetone and oxidation of styrene over Au_{25}/TiO_2, Au_{25}/Fe_2O_3, Au_{25}/HAP and Au_{25}/SiO_2 catalysts [4,14,15]. These metal oxide supports (TiO_2, HAP and Fe_2O_3) have a strong electron-donating tendency [34,35]. The electron transfer from the metal oxide support to gold promotes H_2 activation [36]. In contrast, the inert SiO_2 support has no electron-donating capability, hence, it shows no enhancement in catalytic activity. On the other hand, the activation energy of water-gas shift (WGS) reaction is stable for different supported platinum

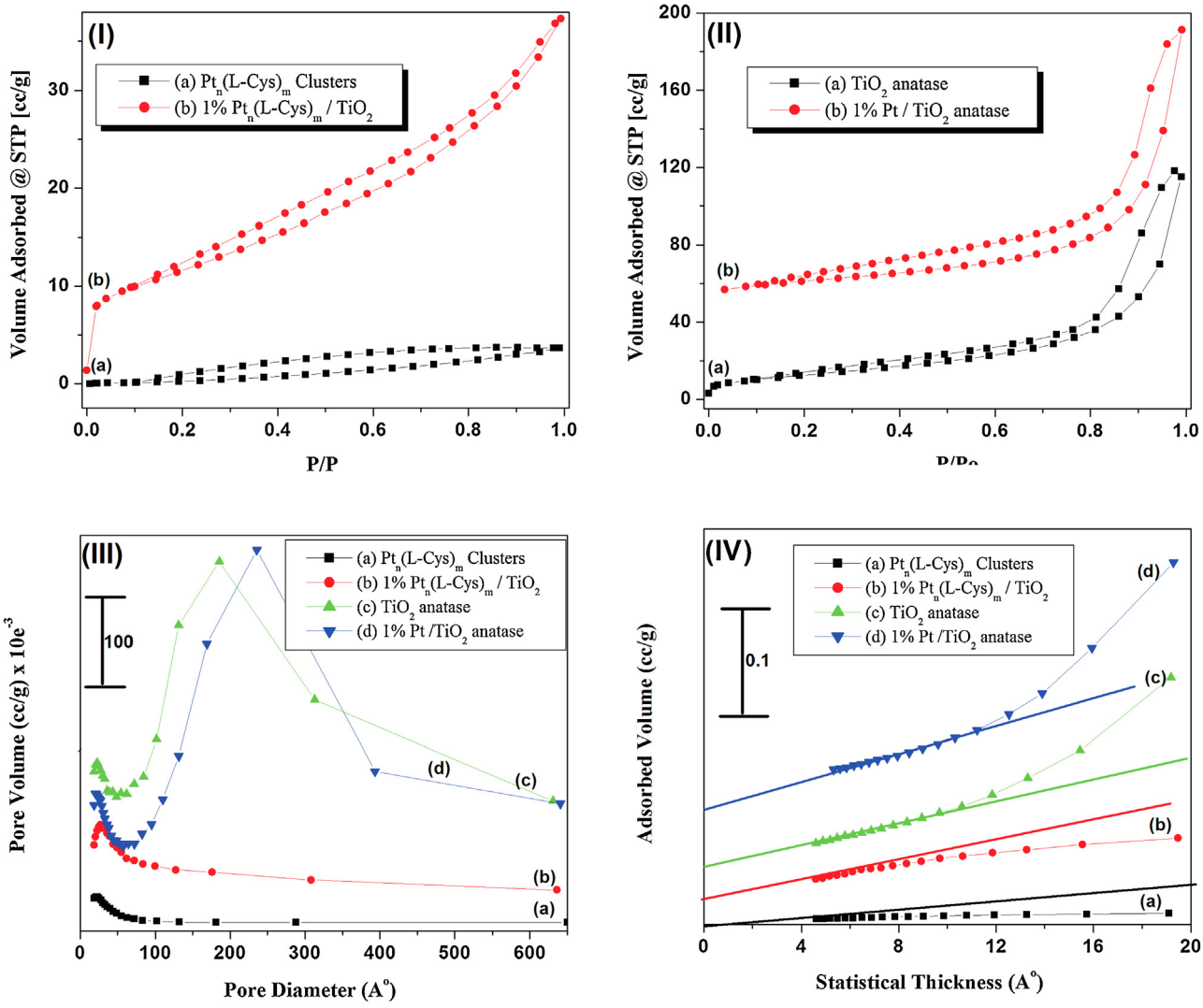

Fig. 5. (I) Nitrogen adsorption–desorption isotherms of synthesized platinum clusters Pt$_n$(L-Cys)$_m$ (curve a) and the supported protected clusters 1% Pt$_n$(L-Cys)$_m$/TiO$_2$, the two isotherms show sorption isotherm from type H2 and H3, respectively. (II) Nitrogen adsorption–desorption isotherms of bare TiO$_2$ (curve a) and 1% Pt/TiO$_2$ catalysts (curve b), the two isotherms show sorption isotherm from type H1. (III) Pore volume distribution curves of all prepared catalysts. (IV) The V_{a-t} plots curves of all prepared catalysts.

Table 2
Texture data obtained from the analysis of nitrogen sorption isotherms of as-prepared clusters catalysts.

No.	Catalysts	S_{BET}(m^2 g^{-1})	S_t(m^2 g^{-1})	Total pore volume(cc g^{-1} × 10^{-3})	Average pore diameter (Å)
1	1% Pt$_n$(L-Cys)$_m$/TiO$_2$anatase	41.07	41.07	59.36	58.26
2	Pt$_n$(L-Cys)$_m$	5.23	5.24	6.67	95.59
3	1% Pt/TiO$_2$ anatase	42.41	42.41	218.24	205.83
4	TiO$_2$ anatase	45.82	45.83	182.76	159.54

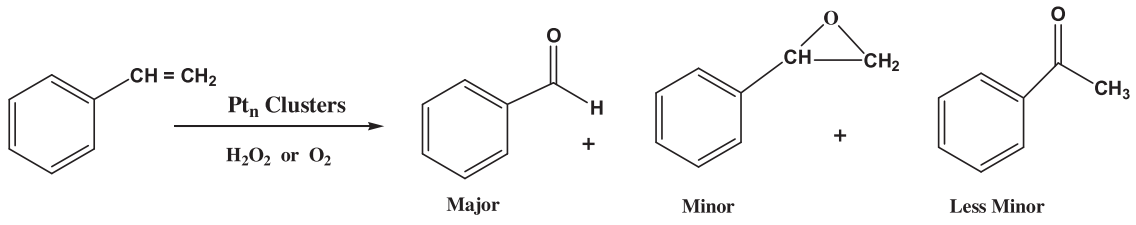

Scheme 1. Catalytic oxidation of styrene over platinum clusters.

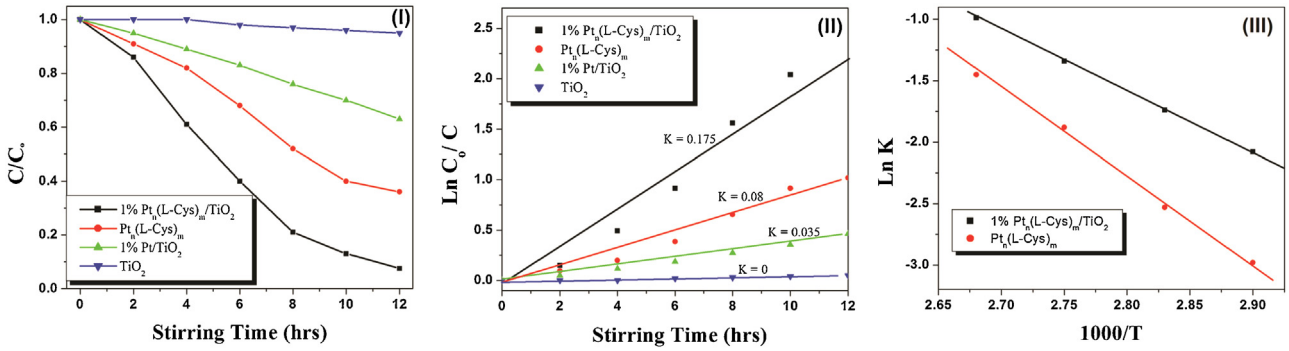

Fig. 6. (I) The change in concentration of styrene with stirring time during the oxidation reaction by H_2O_2 over all prepared catalysts. (II) Ln C_o/C versus stirring time plots, which proof the styrene oxidation reaction, is pseudo-first order. (III) Arrhenius plots, obtained for oxidation of styrene carried out at 70–100 °C over 1% Pt$_n$(L-Cys)$_m$/TiO$_2$ and Pt$_n$(L-Cys)$_m$ catalysts.

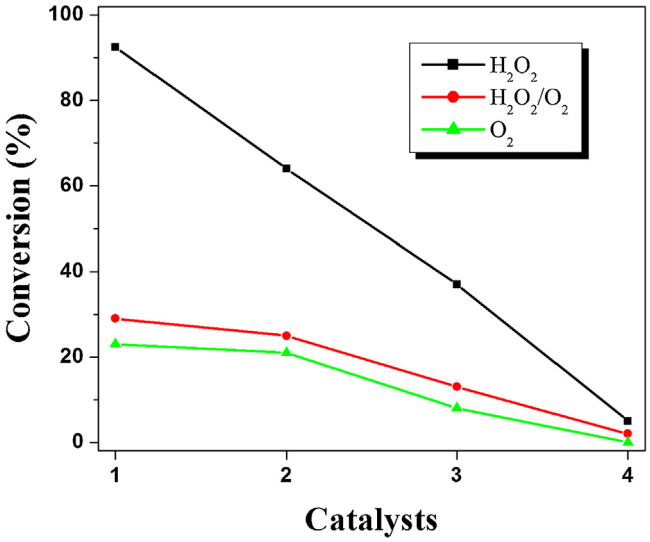

Fig. 7. The catalytic conversion of styrene over all prepared catalysts (1–4) by using different oxidizing agents after 12 h stirring at 80 °C, (1–4) refer to 1% Pt$_n$(L-Cys)$_m$/TiO$_2$, Pt$_n$(L-Cys)$_m$, 1% Pt/TiO$_2$ and TiO$_2$ catalysts, respectively.

catalysts (TiO_2, L-zeolites and mesoporous silica MCM-41) [37]. The apparent activation energy of WGS reaction over Au/TiO_2 catalyst [38] is similar to those reported for gold on ceria, iron oxide, lanthana and other supports [39–43], this confirm the support oxide itself does not participate directly in the WGS reaction.

Fig. 7 shows the relationship between the conversion of styrene and the used oxidizing systems after 12 h stirring. It is clearly observed that system 1 (i.e., H_2O_2 as the oxidant) gives the highest activity in comparison to another two oxidizing systems (Fig. 7). 1% Pt$_n$(L-Cys)$_m$/TiO_2 catalyst shows 92.5% conversion by using H_2O_2 as the oxidant, however by system 2 (H_2O_2 initiator/O_2 oxidant) and system 3 (O_2 as oxidant) shows 29% and 23% conversion, respectively. A similar order of conversion was found for Pt$_n$(L-Cys)$_m$, 1% Pt/TiO_2 and TiO_2 catalysts in the three different oxidant systems (Fig. 7). Therefore, the constituent of the oxidant plays a critical role in the catalytic activity of styrene oxidation.

Benzaldehyde is the major product yield in oxidation of styrene by using the synthesized catalysts whatever the oxidizing agents (Fig. 8). Moreover, the selectivity of benzaldehyde can reach to 100% by using the supported monodisperse clusters (1% Pt$_n$(L-Cys)$_m$/TiO_2) catalyst and H_2O_2 as oxidant or mixture from H_2O_2 (initiator) and O_2 (oxidant) (Fig. 8-I). When oxygen is used as the main oxidant in system 2 and 3 the activity and selectivity of styrene oxidation decrease, which indicates that the oxidizing agent play a big role in oxidation of styrene (Figs. 7 and 8) [15].

To check the advantage of 1% Pt$_n$(L-Cys)$_m$/TiO_2 catalyst and its applicability to reuse [13], the oxidation reaction of styrene was achieved with 100 mg 1% Pt$_n$(L-Cys)$_m$/TiO_2 catalyst and 0.5 ml of hydrogen peroxide as oxidizing agent. Then the catalyst was collected at the end of the reaction and reused for a second cycle and the process repeated so on till four cycles keeping all other parameters constant (Fig. 9). The results revealed that catalyst shows a very good activity for four catalytic runs with a very small loss in the styrene conversion. It can be conclude that the 1% Pt$_n$(L-Cys)$_m$/TiO_2 catalyst possesses high stability and it may be reusable for at least 4 runs, showing a good potential for practical applications (Fig. 9).

The distinct size effect observed for 1% Pt$_n$(L-Cys)$_m$/TiO_2 catalyst in selective oxidation of styrene is interesting. It should be noted that the observed size dependency is not a simple conse-

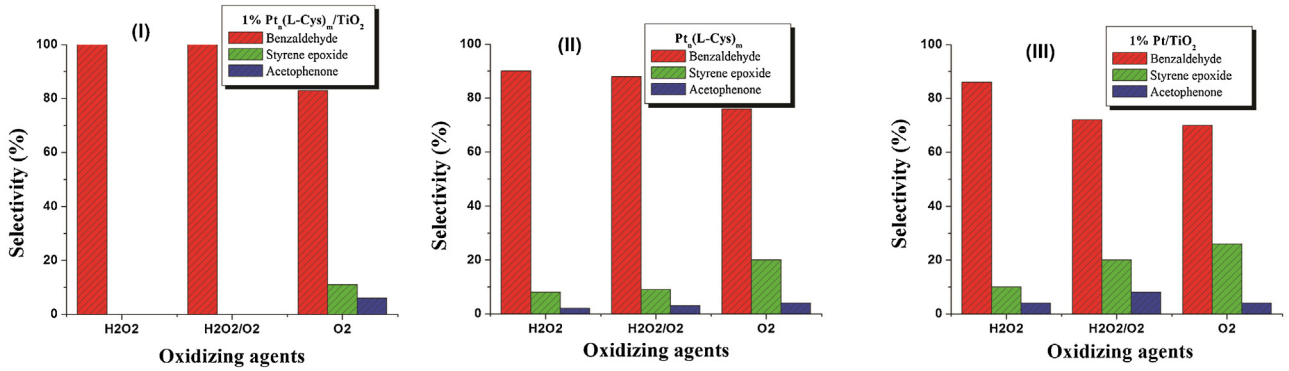

Fig. 8. (I–III) The catalytic selectivity of styrene oxidation products by using different oxidizing agents after 12 h stirring at 80 °C over the prepared catalysts 1% Pt$_n$(L-Cys)$_m$/TiO_2, Pt$_n$(L-Cys)$_m$ and 1% Pt/TiO_2 catalysts, respectively.

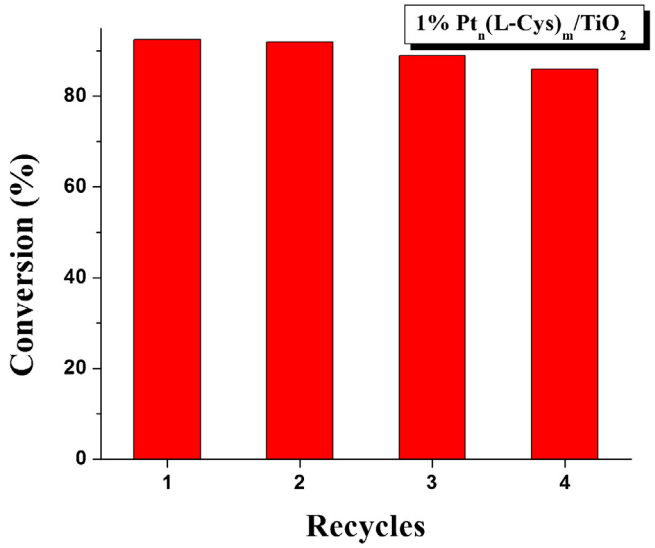

Fig. 9. Repeated cycles of oxidation reaction up to 4 times over 1% Pt_n(L-Cys)$_m$/TiO_2 catalyst by using H_2O_2 as oxidizing agent.

quence of the higher surface area of smaller nanoclusters. I can attribute the extraordinary activity of monodisperse clusters to their electronic properties, which induce HOMU-LUMO gap in their electronic structures [4,44].

Many researchers confirmed that the supported gold catalysts show high activity in epoxidation reactions, this activity attributed to the cationic gold species located at the interface between gold nanoparticles and the reducible supports [45–47]. Density functional theory (DFT) calculations have shown distinct differences in charge distribution on the Au_{13} core (electron-rich) and the Au_{12} shell (electron-deficient) for $Au_{25}(SR)_{18}$ clusters [48–51]. I expect the electronic structures of the synthesized nanoclusters (Pt_n(L-Cys)$_m$) like Au_{25}, moreover, the electronegativity of sulfur atom in ligand is higher than the platinum atom in the surface of clusters (S-Pt). Therefore, I can say there are partial positive charge in the surface platinum atoms and partial negative charge in the sulfur atom. The presence of partial positive charges on the surface Pt atoms in Pt_n(L-Cys)$_m$ clusters should facilitate activation of the nucleophilic group (—CH=CH_2) in styrene since the positive Pt atoms are electrophilic. In contrast, the electron-rich platinum core should facilitate O_2 activation.

4. Conclusion

In this work I present a new synthesis method to prepare monodisperse platinum clusters protected by L-cysteine. This method can produce a very narrow size distribution platinum clusters ~1 nm. The optical properties of the prepared clusters were studied by UV–vis spectroscopy. The platinum nanoclusters anchored to the ligand through the thiol group, which confirmed by disappearance of S—H vibrational band at 2535–2570 cm^{-1} in IR spectra of clusters. The metal-to-ligand ratio (M/L) and the average chemical formula of the prepared clusters were calculated from thermogravimetric analysis (TGA) and elemental analysis (EA). The particle sizes of all synthesized catalysts were assessed by transmission electron microscopy (TEM) and powder X-ray diffraction analysis (XRD. The complete isotherm of the prepared clusters was measured using nitrogen adsorption–desorption at −196 °C, specific surface area S_{BET}, pore volume and average pore diameter were calculated. To study the catalytic activity of synthesized clusters, oxidation of styrene is used as a model reaction to demonstrate that. Supported monodisperse platinum clusters (1% Pt_n(L-Cys)$_m$/TiO_2) showed extremely catalytic activity in oxidation of styrene with 100% benzaldehyde selectivity. Polydisperse platinum metal clusters over TiO_2 was prepared to comparison between the catalytic activity of monodisperse clusters and polydisperse clusters. The core/shell nature of the protected platinum clusters, i.e., the presence of a surface layer of platinum atoms bearing partial positive charges and the electron-rich core, is believed to be primarily responsible for their catalytic activities. H_2O_2 as oxidizing agent can achieve the oxidation of styrene even with monodisperse and polydisperse platinum clusters by high conversion and selectivity more than oxygen gas. The role of support is not only better disperse of platinum clusters but also reduce the activation energy of styrene oxidation reaction

Acknowledgments

This work is supported by Assiut University, Egypt. I kindly acknowledge Prof. Dr. H. Gasteiger for carrying out TGA measurement in technical university of Munich (TUM), Germany.

Appendix A. Supplementary data

Supplementary data associated with this article can be found, in the online version, at http://dx.doi.org/10.1016/j.molcata.2015.12.011.

References

[1] M. Haruta, Nature 437 (2005) 1098.
[2] A.S.K. Hashmi, G.J. Hutchings, Angew. Chem. Int. Ed. 45 (2006) 7896.
[3] J. Luo, V.W. Jones, M.M. Maye, L. Han, N.N. Kariuki, C.-J. Zhong, J. Am. Chem. Soc. 124 (2002) 13988.
[4] B.Y. Zhu, H. Qian, M. Zhu, R. Jin, Adv. Mater. 22 (2010) 1915–1920.
[5] S. Kunz, K. Hartl, M. Nesselberger, F. Schweinberger, G. Kwon, M. Hanzlik, K. Mayrhofer, U. Heiz, M. Arenz, Phys. Chem. Chem. Phys. 12 (2010) 10288–10291.
[6] Z. Wu, J. Suhan, R. Jin, J. Mater. Chem. 19 (2009) 622–626.
[7] H. Qian, Y. Zhu, R. Jin, Nano 3 (2009) 3795–3803.
[8] H. Qian, R. Jin, Nano Lett. 9 (2009) 4083–4087.
[9] M. Farrag, M. Tschur, U. Heiz, Chem. Mater. 25 (2013) 862.
[10] M. Farrag, M. Tschurl, A. Dass, U. Heiz, Phys. Chem. Chem. Phys. 15 (2013) 12539.
[11] S. Kunz, P. Schreiber, M. Ludwig, M.M. Maturi, O. Ackermann, M. Tschurl, U. Heiz, Phys. Chem. Chem. Phys. 15 (2013) 19253.
[12] I. Schrader, J. Warneke, J. Backenköhler, S. Kunz, J. Am. Chem. Soc. 137 (2015) 905–912.
[13] M. Farrag, J. Photochem. Photobiol. A: Chem. 318 (2016) 42–50.
[14] Y. Zhu, H. Qian, B.A. Drake, R. Jin, Angew. Chem. Int. Ed. 49 (2010) 1295–1298.
[15] Y. Zhu, H. Qian, R. Jin, Chem. Eur. J. 16 (2010) 11455–11462.
[16] S. Lubis, L. Yuliati, S. Ling Lee, I. Sumpono, H. Nur, Chem. Eng. J. 209 (2012) 486–493.
[17] O.S. Mohamed, S.A. Ahmed, M.F. Mostafa, A.A. Abdel-Wahab, Int. J. Photoenergy 2008 (2007) 1–11, Article ID 205358.
[18] Y. Liu, H. Tsunoyama, T. Akita, T. Tsukuda, Chem. Commun. 46 (2010) 550–552.
[19] M. Turner, V.B. Golovko, O.P.H. Vaughan, P. Abdulkin, A. Berenguer-Marcia, M.S. Tikhov, B.F.G. Johnson, R.M. Lambert, Nature 454 (2008) 981.
[20] M. Farrag, M. Thämer, M. Tschurl, T. Bürgi, U. Heiz, J. Phys. Chem. C 116 (2012) 8034.
[21] B.Z. Wu, J. Chen, R. Jin, Adv. Funct. Mater. 21 (2011) 177.
[22] J.A. Creighton, D.G. Eadon, J. Chem. Soc. Faraday Trans. 87 (1991) 3881–3891.
[23] S. Chen, K. Kimura, J. Phys. Chem. B 105 (2001) 5397–5403.
[24] M.J. Hostetler, J.E. Wingate, C.-J. Zhong, J.E. Harris, R.W. Vachet, M.R. Clark, J.D. Londono, S.J. Green, J.J. Stokes, G.D. Wignall, G.L. Glish, M.D. Porter, N.D. Evans, R.W. Murray, Langmuir 14 (1998) 17–30.
[25] E.S. Shibu, M.A. Habeeb Muhammed, T. Tsukuda, T. Pradeep, J. Phys. Chem. C 112 (2008) 12168.
[26] R. Sharma, L.-S. Bouchard, Sci. Rep. 2 (2012) 277.
[27] T. Hyde, Platinum Met. Rev. 52 (2008) 129–130.
[28] A. Zielinska-Jurek, A. Zaleska, Catal. Today 230 (2014) 104–111.
[29] A. Neren Ökte, Appl. Catal. A: Gen. 475 (2014) 27–39.
[30] I.U.P.A.C. Recommendations, Pure Appl. Chem. 66 (1994) 1739.
[31] M.T.h. Makhlouf, B.M. Abu-Zied, T.H. Mansoure, Appl. Surf. Sci. 274 (2013) 45–52.
[32] W.M. Shaheen, A.A. Zahran, G.A. El-Shobaky, Colloids Surf. A: Physicochem. Eng. Asp. 231 (2003) 51–65.
[33] Y. Zhu, H. Qian, B.A. Drake, R. Jin, Angew. Chem. 122 (2010) 1317–1320.

[34] M. Boronat, F. Illas, A. Corma, J. Phys. Chem. A. 113 (2009) 3750–3757.
[35] P. Winiarek, J. Kijenski, J. Chem. Soc. Faraday Trans. 94 (1998) 167–172.
[36] P. Clause, A. Bruckner, C. Mohr, H. Hofmeister, J. Am. Chem. Soc. 122 (2000) 11430–11439.
[37] M. Yang, J. Liu, S. Lee, B. Zugic, J. Huang, L.F. Allard, M. Flytzani-Stephanopoulos, J. Am. Chem. Soc. 137 (2015) 3470–3473.
[38] M. Yang, L.F. Allard, M. Flytzani-Stephanopoulos, J. Am. Chem. Soc. 135 (2013) 3768–3771.
[39] Q. Fu, H. Saltsburg, M. Flytzani-Stephanopoulos, Science 301 (2003) 935.
[40] Q. Fu, W. Deng, H. Saltsburg, M. Flytzani-Stephanopoulos, Appl. Catal. B 56 (2005) 57.
[41] M.B. Boucher, S. Goergen, N. Yi, M. Flytzani-Stephanopoulos, Phys. Chem. Chem. Phys. 13 (2011) 2517.
[42] W.D. Williams, M. Shekhar, W.S. Lee, V. Kispersky, W.N. Delgass, F.H. Ribeiro, S.M. Kim, E.A. Stach, J.T. Miller, L.F. Allard, J. Am. Chem. Soc. 132 (2010) 14018.
[43] J.D. Lessard, I. Valsamakis, M. Flytzani-Stephanopoulos, Chem. Commun. 48 (2012) 4857.
[44] M. Zhu, C.M. Aikens, F.J. Hollander, G.C. Schatz, R. Jin, J. Am. Chem. Soc. 130 (2008) 5883.
[45] N.S. Patil, B.S. Uphade, P. Jana, R.S. Sonawane, S.K. Bhargava, V.K. Choudhary, Catal. Lett. 94 (2004) 89.
[46] E.E. Stangland, K.B. Stavens, R.P. Andres, W.N. Delgass, J. Catal. 191 (2000) 332.
[47] A. Abad, P. Concepcion, A. Corma, H. Garcia, Angew. Chem. Int. Ed. 44 (2005) 4066.
[48] J. Akola, M. Walter, R.L. Whetten, H. Hakkinen, H. Gronbeck, J. Am. Chem. Soc. 130 (2008) 3756.
[49] M. Walter, J. Akola, O. Lopez-Acevedo, P.D. Jadzinsky, G. Calero, C.J. Ackerson, R.L. Whetten, H. Grönbeck, H. Hákkinen, Proc. Natl. Acad. Sci. U. S. A. 105 (2008) 9157.
[50] M. Zhu, C.M. Aikens, M.P. Hendrich, R. Gupta, H. Qian, G.C. Schatz, R. Jin, J. Am. Chem. Soc. 131 (2009) 2490.
[51] C.M. Aikens, J. Phys. Chem. C 112 (2008) 19797.